Hindawi
Geofluids
Volume 2022, Article ID 6211437, 19 pages
https://doi.org/10.1155/2022/6211437

Research Article

Thermal Response and Mechanical Behaviors of Compact Basalts Induced by Microwave Irradiation

Xiao-Wu Zhang,[1,2] **Jin-Hai Xu**,[1,2] **Liang Chen**,[1,2] **Yue Cao**,[1,2] **Lei Sun**,[1,2] **and Faiz Shaikh**[3]

[1]*State Key Laboratory of Coal Resources and Safe Mining, School of Mines, China University of Mining and Technology, Xuzhou, China*
[2]*School of Mines, China University of Mining and Technology, Xuzhou, China*
[3]*School of Civil and Mechanical Engineering, Curtin University, Perth, Australia*

Correspondence should be addressed to Xiao-Wu Zhang; tb20020039b0@cumt.edu.cn

Received 17 June 2022; Accepted 24 August 2022; Published 5 September 2022

Academic Editor: Jinpeng Zhang

Microwave pretreatment could be an invaluable method to improve the efficiency of the rock breakage in the excavation and comminution operations. To investigate the influence of microwave irradiation on the thermal response and mechanical behavior of compact rocks, a series of physical and mechanical experiments were conducted on the nontreated and treated basalts. The mineral compositions of the basalts were obtained by X-ray diffraction (XRD) test. Scanning electron microscope (SEM) images and geological sketch were utilized to analyze the propagation pattern of the microcracks and macrofractures caused by the microwave irradiation. High power density microwave can induce the complication of the microcracks and exchange the pattern of the macrofracture network. Based on the uniaxial compression strength (UCS) test, the mechanical performance of the basalts was evidently reduced with the increase of the microwave power and exposure time. The experimental results prove that microwave-assisted method has significant potential application to preweakening rocks in civil and mining engineering.

1. Introduction

The growing demand for civil and mining engineering, constantly excavation and mining activities will place a strain on the construction efficiency of tunneling and drilling in the future. In an effort to address this challenge, mechanical rock fragmentation mainly based on tunnel boring machines (TBMs) was widely applicated in the tunneling and mining operations in recent decades [1]. Comparing with conventional drilling and blasting methods, the mechanical approach has advantages in higher advance rates, better excavation profile, and less support requirement [2–4]. However, the performance of TBMs could significantly compromised if unfavorable geological conditions were encountered [5]. Of the awful geological conditions, extremely hard and abrasive rocks (especially, uniaxial compression strength over 200 MPa) emerge as one of the greatest challenges, which leads shield machines and TBMs were subjected to high cutter wear rate and difficulty in cutter change-out [6]. As a result, new and effectively solutions were impatiently required to preweakening rock strength, prolong the mechanical life, and improve the productivity of rock breaking process.

Formation heat treatment (FHT) technology was first presented as a novel concept in 1995 [7]. A few years later, the newly proposed method was tested in a conventional sandstone gas well by using an intense electrical heater to degrade clay minerals and to create macrofractures. Fortunately, the field test was completely successful and demonstrated the FHT to be a feasible approach to preweakening rocks [8, 9]. After that, a series of preweakening rock methods (e.g., laser technology [10–12], plasma blasting [13], and electric pulses [14–16]) were widely applied in the oil and mining industry to preweakening hard rock hardness by inducing microcracks within them. In these conventional methods, heat is transferred

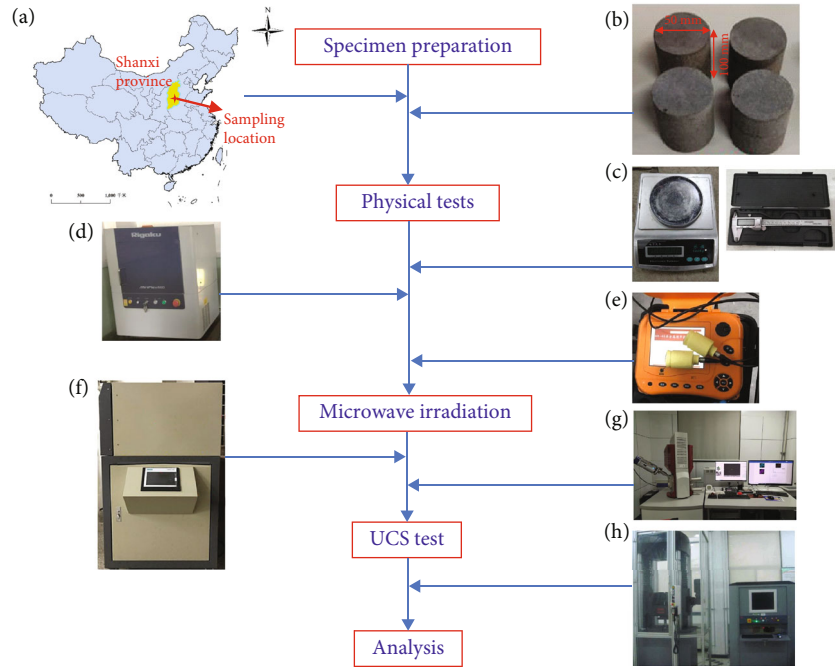

Figure 1: Experimental procedures and equipment: (a) sampling site, (b) parts of the cylindrical specimens, (c) mass and dimension measurement, (d) XRD devices, (e) ultrasonic wave instrument, (f) microwave treatment system, (g) SEM devices, and (h) UCS system.

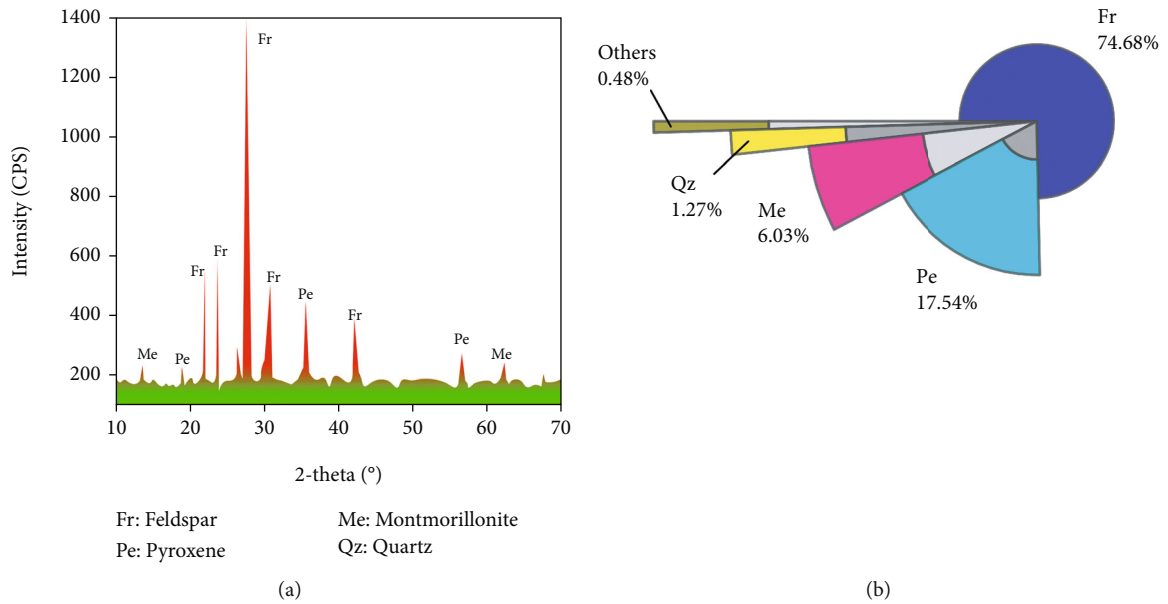

Figure 2: XRD test of the basalts: (a) mineralogic composition and (b) proportion of the minerals.

Table 1: Physical properties of the testing basalt specimen.

Size Length/mm	Diameter/mm	Mass/g	Density/(g/cm^3)	P-wave/(m/s)
100 ± 0.3	50 ± 0.2	2095.73 ± 13.24	3.684 ± 0.3	5703.46 ± 56

by thermal conduction and convection, which could be significantly influenced by the geology formation (e.g., aquicludes and faults). Therefore, to eliminate such disadvantages, microwave treatment as a promising approach for fracturing and breaking rocks has attracted extensive attention in recent decades [17]. When exposed to

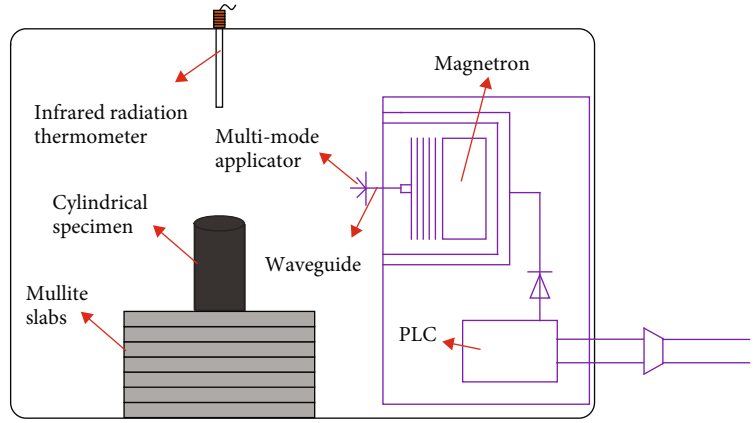

Figure 3: Schematic of microwave irradiation system.

Table 2: Testing results of ultrasonic wave velocity induced by microwave irradiation.

Power/kW	Exposure time/s	P-wave velocity/(m/s)	Mean value/(m/s)	Absolute deviation	Relative deviation (%)	Standard deviation/(m/s)	Coefficient of variation (%)
		5783.26		52.4567	0.9153		
Nontreated	0	5767.12	5730.81	36.3167	0.6337	44.7247	0.7804
		5642.03		88.7733	1.5491		
		5324.95		67.9833	1.2932		
	60	5267.48	5256.97	2.6800	0.0509	36.6391	0.6970
		5178.47		86.3300	1.6398		
		4321.57		41.4500	0.9684		
1	150	4259.48	4280.12	20.6400	0.4822	16.9219	0.3954
		4259.31		20.8100	0.4862		
		3544.15		39.9833	1.1410		
	300	3508.94	3504.17	4.7733	0.1362	20.0682	0.5727
		3459.41		44.7567	1.2772		
		4925.78		52.4567	0.9153		
	30	4748.37	4856.51	36.3167	0.6337	44.7247	0.9209
		4895.37		88.7733	1.5491		
		4458.49		69.2733	1.4264		
3	50	4357.42	4321.81	108.1367	2.2266	74.2618	1.7183
		4149.52		38.8633	0.8002		
		3746.84		136.6800	3.1626		
	90	3601.79	3687.04	35.6100	0.8240	35.7317	0.9691
		3712.48		172.2900	3.9865		
		5346.59		88.7733	1.5491		
	10	5206.78	5264.80	81.7900	1.5535	34.3500	0.6524
		5241.03		58.0200	1.1020		
		4655.13		23.7700	0.4515		
5	20	4579.45	4611.01	44.1167	0.9568	18.5595	0.4025
		4598.46		31.5633	0.6845		
		4126.79		12.5533	0.2722		
	30	4103.48	4107.59	19.2033	0.4675	8.2566	0.2010
		4092.49		4.1067	0.1000		

microwave irradiation, natural and induced dipoles in rocks rotate hundreds of millions of times per second with the alternation of the electromagnetic field of microwave. Microwave energy is rapidly converted into heat through fierce friction between molecules, which results in overall temperature increase [18, 19]. Comparing with traditional

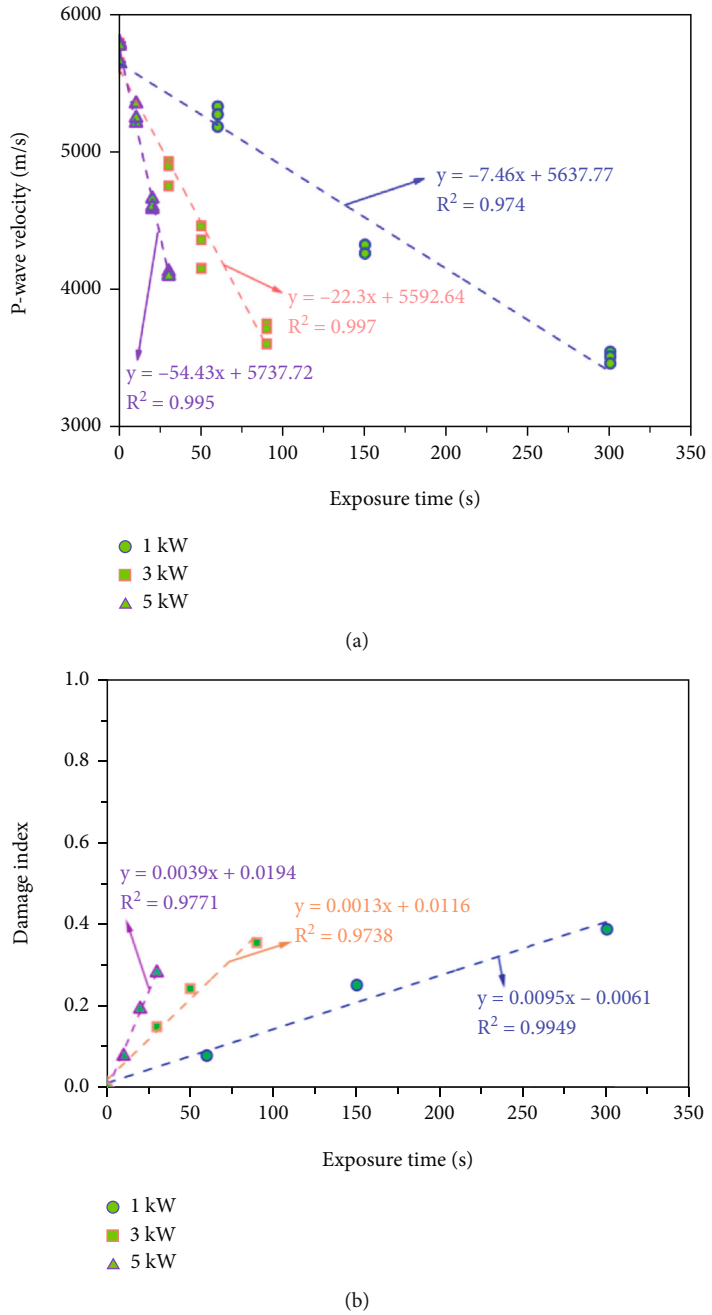

Figure 4: Ultrasonic wave propagation induced by microwave irradiation: (a) velocity of P-wave and (b) damage index based on the P-wave.

FHT methods, microwave irradiation could heat the interior and exterior of rocks simultaneously. Additionally, when absorbing the same heat, different types of minerals expand at different rates, which has been shown to depend on the dielectric, thermal, and mechanical properties of the minerals involved [20, 21]. This means that microwave irradiation could generate thermal stresses between well microwave absorbers and weak microwave absorbers to break rocks efficiently. Therefore, microwave precondition method has the advantages of rapid heating, selective heating, and volumetric heating that are very suitable for application in tunneling and mining operations.

In recent decades, several researchers have investigated the influence of microwave irradiation on the physical and mechanical properties of rocks. Ferri et al. [22] experimental investigated the effect of on temperature profiles and strength reduction of different types of hard rocks induced by microwave irradiation for a range of exposure times and microwave power levels. The authors reported that the tensile and uniaxial compressive strengths of rocks were reduced with increasing exposure time and power level. Lu et al. [23] experimentally studied the computed tomography and acoustic emission (AE) characteristics of basalt rock subjected to microwave irradiation. They reported that the

Table 3: Testing results of surface temperature induced by microwave irradiation.

Power/kW	Exposure time/s	Temperature/(°C)	Mean value/(°C)	Absolute deviation	Relative deviation (%)	Standard deviation/(°C)	Coefficient of variation (%)
		23.04		0.7800	3.2746		
Nontreated	0	24.84	23.82	1.0200	4.2821	0.4354	1.8280
		23.58		0.2400	1.0076		
		73.61		1.1800	1.6292		
	60	73.49	72.43	1.0600	1.4635	0.9149	1.2632
		70.19		2.2400	3.0926		
		126.84		3.5700	2.8961		
1	150	123.91	123.27	0.6400	0.5192	1.8523	1.5026
		119.06		4.2100	3.4153		
		200.09		2.8500	1.4449		
	300	196.15	197.24	1.0900	0.5526	1.1742	0.5953
		195.48		1.7600	0.8923		
		79.52		0.8933	1.1362		
	30	76.51	78.63	2.1167	2.6920	0.8676	1.1035
		79.85		1.2233	1.5559		
		129.16		8.3967	6.9530		
3	50	117.16	120.76	3.6033	2.9838	3.4394	2.8480
		115.97		4.7933	3.9692		
		198.49		2.3933	1.2205		
	90	196.31	196.10	0.2133	0.1088	1.1817	0.6026
		193.49		2.6067	1.3293		
		46.95		2.0367	4.5347		
	10	45.21	44.91	0.2967	0.6605	1.0371	2.3091
		42.58		2.3333	5.1952		
		78.49		1.6700	2.1739		
5	20	77.95	76.82	1.1300	1.4710	1.1502	1.4972
		74.02		2.8000	3.6449		
		110.29		1.9833	1.8312		
	30	109.62	108.31	1.3133	1.2126	1.3551	1.2512
		105.01		3.2967	3.0438		

degree of crack propagation in the basalt increases with the microwave irradiation time. Lu et al. [24] conducted true triaxial tests of sandstone under different microwave irradiation conditions. The authors reported that the strength of the treated sandstone was significantly lower than that of the nontreated specimen and shows first increased and then decreased variation trend. Zhao et al. [25] experimentally preformed a series of laboratory tests to investigate the weakening effect of microwave irradiation on granite. They reported that the weakening mechanism is mainly related to the differential expansion among mineral particles and the microcracks generated in the rocks. Ge and Sun [26] carried on AE test to investigate the evolution of different types of cracks in gabbro subjected to uniaxial compression loads. The authors reported that the amount of microcracks in gabbro increases and AE becomes more and more active after microwave irradiation. Xu et al. [27] employ experimental and numerical methods to investigate the fracture formation process and the damage of rock induced by microwave radiation. The authors proposed three damage indicators under microwave irradiation, namely, P-wave velocity attenuation, temperature distribution, and fracture pattern, which were a substantial influence by the microwave power and irradiation time. Zhao et al. [28] experimentally investigated the heating characteristics of various igneous rock-forming minerals after microwave irradiation. They reported that the heating characteristics of minerals that are significantly influenced by their microwave sensitivities are the basis of the weakening effect of microwave irradiation on rock. Sair et al. [29] carried out a series of uniaxial compressive strength (UCS) and Brazilian tensile strength (BTS) tests on the nontreated and treated igneous rocks. The authors reported that the mechanical strength of igneous rocks was significantly influenced by microwave irradiation depending on the applied energy, the exposure time, and mineralogy.

In this research, the influence of microwave irradiation, at different microwave power settings and exposure time, on thermal response and mechanical behavior of

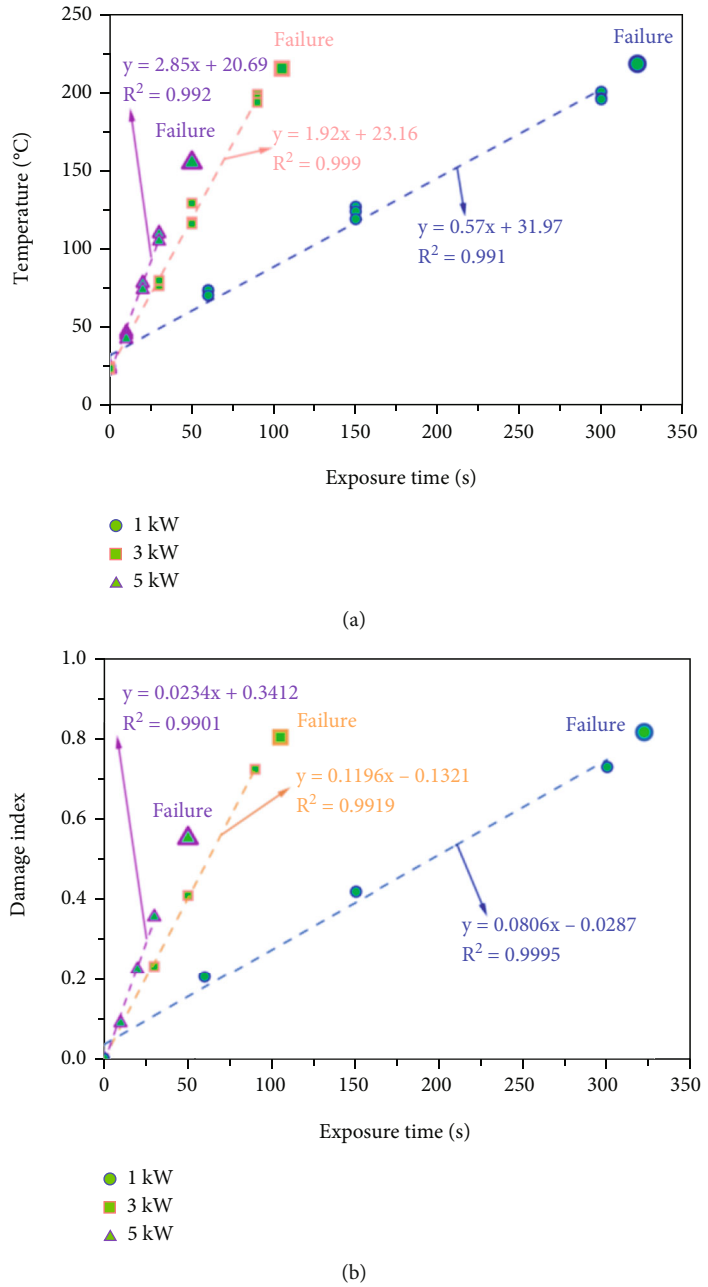

Figure 5: Thermal response induced by microwave irradiation: (a) surface temperature of the basalts and (b) damage index based on the surface temperature.

the compact basalts is experimentally investigated by using a multimode industrial microwave system with a frequency of 2.45 GHz. Then, conventional UCS test was conducted to analyze the degradation of the mechanical performance of the basalts after microwave irradiation. In addition, the morphology of the microcracks and macrofracture propagation pattern was researched by SEM pictures and geological sketches. The experimental results could provide a further understanding of the fractures propagation mechanisms induced by microwave irradiation and demonstrate that microwave treatment could be an effective and efficient method to preweakening the overall strength of the hard and abrasive rocks.

2. Materials and Methodology

A series of physical and mechanical tests (e.g., ultrasonic wave test, X-ray diffraction (XRD) test, scanning electron microscope (SEM), and UCS test) were conducted on the nontreated and treated basalts to investigate the influence of microwave irradiation on the thermal response and mechanical behavior of compact rocks. The complete experimental procedures and equipment used in this research were demonstrated in Figure 1.

2.1. Specimen Preparation. Basalts are extremely packed plutonic rocks which are the main constituent of the Earth's

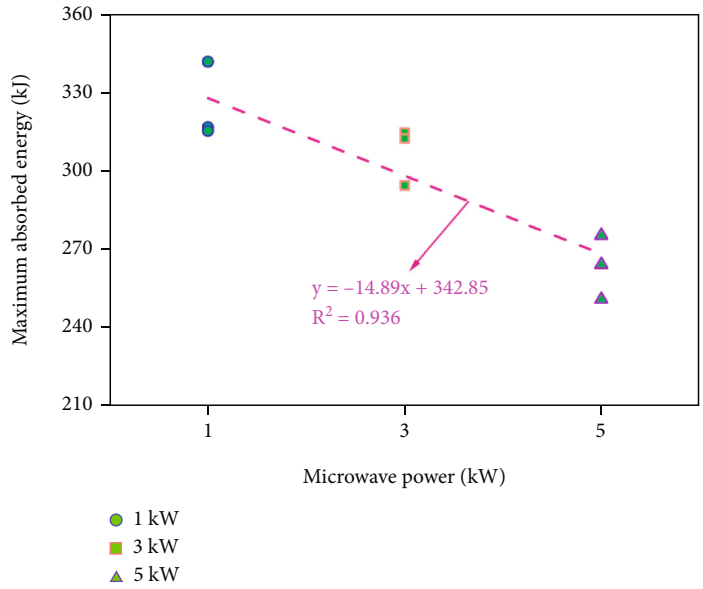

Figure 6: The maximum absorbed microwave energy versus microwave power levels.

oceanic and continental crust. Compact basalts present a high uniaxial compression strength (UCS), usually higher than 300 MPa, and are a well microwave absorber. Thus, compact basalts are selected to investigate the effect of microwave irradiation on the thermal response and mechanical behaviors of the compact rocks.

The intact basalt block, from Shanxi province, China, was cored into standard cylindrical specimens with 50 mm in diameter and 100 mm in height, following the suggestion of the International Society of Rock Mechanics and Rock Engineering (ISRM) [30]. The sampling location of the basalts and parts of cylindrical specimens for testing was shown in Figure 1(b). All the prepared basalt specimens were free from visible macrocracks and large grain intrusions. Before testing, specimens were dried in an oven at 60°C for 48 h and naturally cooled down to room temperature to eliminate the influence of moisture.

2.2. Mineralogy. Any kind of crystalline substance has its own peculiarity X-ray diffraction (XRD) spectrum, which is not influenced by the involvement of other substances. Thus, the complex composited materials can be reflected by a series of XRD spectrums based on the type of the mineral substance. By comparing the crystal plane spacing and intensity in the XRD spectrum with the ICCD International Powder Diffraction Database, the type of the material's compositions and their proportions were obtained. Prior to the microwave irradiation, thin sections of the basalts were prepared for XRD analysis to detect mineralogical components. The XRD spectrum of the specimen (as shown in Figure 2) indicates that the basalts mainly consist of 74.68% feldspar, 17.54% pyroxene, 6.03% montmorillonite, and 1.27% quartz.

2.3. Physical Property Tests. Pilot experiments, such as mass measurement, volume determination, and ultrasonic tests, were conducted according to ASTM standards and ISRM suggested methods. Smooth-cut specimens were used for the determination of densities. The specimen volumes were calculated from the recorded values by a conventional caliper. A balance with capability of weighing to an accuracy of 0.01 g was utilized to capture the mass of the specimens. The density was obtained from the ratio of the specimen mass to the specimen volume. Moreover, to ensure the homogeneity of the basalts, P-wave velocity tests were performed by using the NN-4B ultrasonic measure instrument (as shown in Figure 1(e)) at room temperature. The physical testing results of unirradiated specimens are listed in Table 1.

2.4. Microwave Irradiation Tests. Microwave is an electromagnetic wave with a frequency from 300 MHz to 3 GHz and a wavelength from 1 mm to 1 m. The frequency commercially used in the microwave ovens and industrial microwave systems is 915 MHz or 2.45 GHz. Specifically, a multimode industrial microwave system with a frequency of 2.45 GHz was utilized to thermally treat the basalt specimens in the study. The microwave irradiation system (as shown in Figure 1(f)) consists of the microwave generator, control system, monitoring system, and a closed cavity. The magnetrons installed in the microwave generator which are controlled by the programmable logic controller (PLC) generate microwave from 0.1 to 6 kW power. In addition, an infrared radiation thermometer installed in the center of the cavity's roof can measure the surface temperature of the specimen, and a handheld infrared gun with a range of 45°C ~1200°C was employed to assist the temperature measurement. The basalt specimens for microwave irradiation were placed in an optimized position, which had a distance approximate of 15 cm to the microwave applicator. A bedding cushion consists of several mullite slabs which was a weak microwave absorber were utilized to ensure the testing basalts homogeneous exposed. The functional diagram of microwave irradiation system was shown in Figure 3.

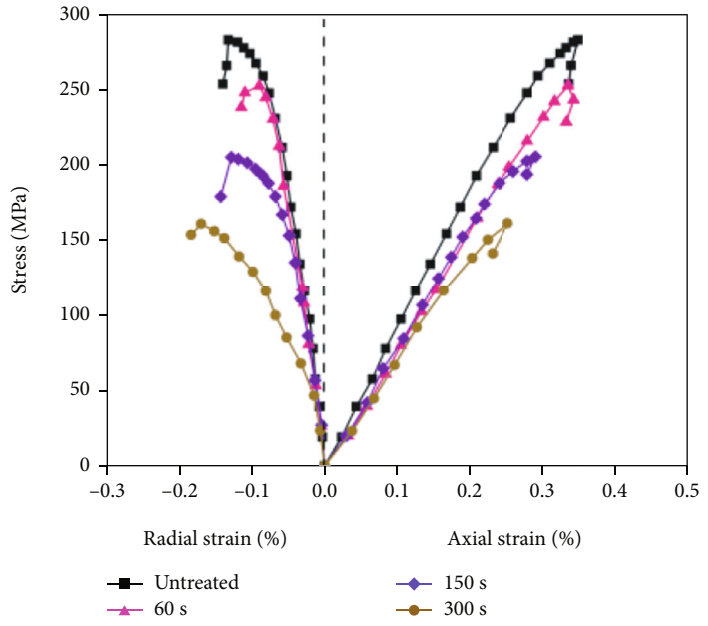

(a)

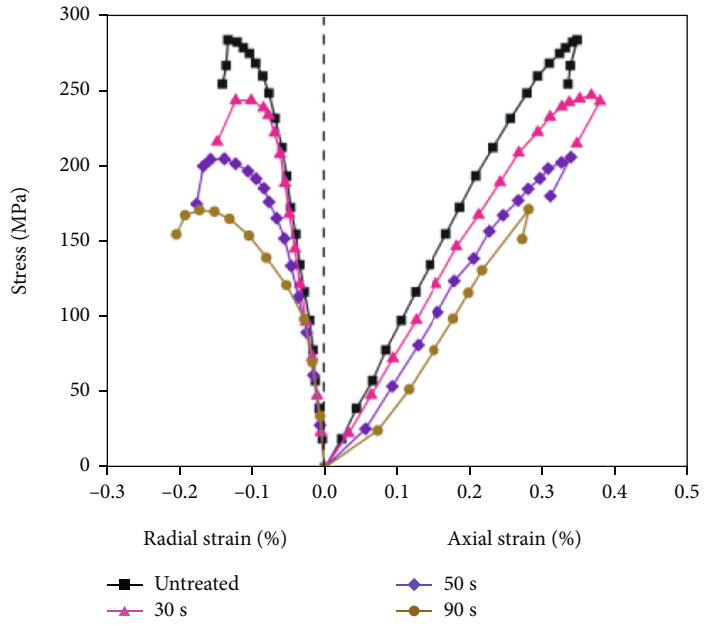

(b)

Figure 7: Continued.

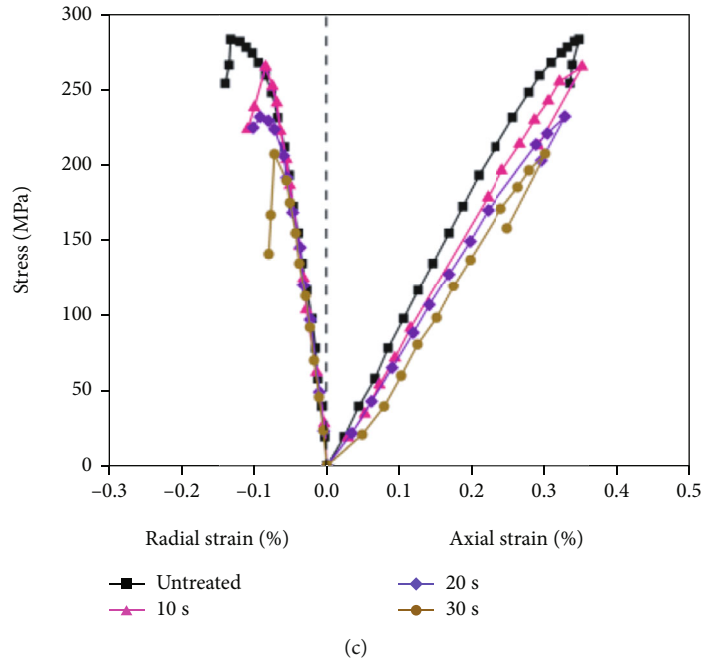

(c)

Figure 7: Stress-strain curve of the basalts before and after microwave irradiation: (a) power density is 1 kW; (b) power density is 3 kW; (c) power density is 5 kW.

Three power levels (1 kW, 3 kW, and 5 kW) of the microwave were applied to the basalts. Specially, the maximum exposure time of the basalts treated at the 1 kW, 3 kW, and 5 kW power before the rocks fragmentized was about 320 s, 100 s, and 50 s, respectively. Therefore, for 1 kW power level, the microwave exposure time was set to 60 s, 150 s, and 300 s; for 3 kW power level, the microwave exposure time was set to 30 s, 50 s, and 90 s; for 5 kW power level, the microwave exposure time was set to 10 s, 20 s, and 30 s.

2.5. UCS Tests. The conventional UCS tests were performed on both nontreated and treated basalt specimens by using a MTS-4000 rigid servo-controlled triaxial compression test system with a loading capacity of 2200 KN (as shown in Figure 1(h)). The compression test system could be able to makes real-time recording of the axial displacement when the load applied to the specimen and a radial linear variable differential transducer which wrapped tightly around the specimen was employed to monitor the radial deformation. The loading pattern was set to load control at a rate of 0.2 mm/min. To avoid discreteness of test results as possible, the UCS tests of the nontreated and treated basalts were both repeated in triplicate, and test results in the study were expressed as mean value.

3. Results

3.1. Ultrasonic Wave Propagation. Ultrasonic wave test is the most convenient and intuitive method to assess the quantity of the microcracks in the material. The microcracks existed in the rocks is able to cause the refraction and diffraction of the ultrasonic wave. Thus, the more the microcracks in the rocks, the lower transmission velocity of the ultrasonic wave. The testing results of the P-wave velocity of the basalts induced by microwave irradiation were listed in Table 2. To illustrate the P-wave velocity of the basalts visually, the P-wave velocity of the basalt specimen as a function of the microwave exposure time was shown in Figure 4(a). The P-wave velocity of the treated basalts decreases gradually with the increasing exposure time, and the dependence of the P-wave velocity on the irradiation time can be characterized by a straight line. In addition, high power density microwave can induce more microcracks in the basalts and decrease the velocity of P-wave more seriously.

Damage index is a curtail parameter to assess the degree of the deformation and failure of rocks subjected to the microwave irradiation. The damage index based on the velocity of the P-wave induced by the microwave irradiation can be calculated as follows:

$$D_w = \frac{v_0 - v_i}{v_0}, \tag{1}$$

where D_w is the damage index based on the velocity of the P-wave; v_0 is the P-wave velocity of the basalts nontreated by the microwave; v_i is the P-wave velocity of the basalts treated by the microwave. Figure 4(b) illustrated the damage index based on the P-wave velocity of the basalts induced by the microwave irradiation. It can obtain that the damage degree of the basalts induced by the microwave irradiation increases with the elapsed exposure time. Additionally, by comparing the slopes of the fitting curves, the damage degree of the basalts increases rapidly when exposed by high power of microwave. Finally, the maximum of the damage index of the basalts induced by the 1 kW, 3 kW and 5 kW was 0.39, 0.35, and 0.28, respectively, all of which were below 0.4. It indicated that the value of damage index based on the P-wave velocity induced by the microwave irradiation was less than 0.4.

Table 4: Testing results of UCS induced by microwave irradiation.

Power/kW	Exposure time/s	UCS/(MPa)	Mean value/(MPa)	Absolute deviation	Relative deviation (%)	Standard deviation/(MPa)	Coefficient of variation (%)
		289.49		6.9367	2.4550		
Nontreated	0	278.49	282.55	4.0633	1.4381	2.8457	1.0072
		279.68		2.8733	1.0169		
		255.48		2.8033	1.1095		
	60	250.06	252.68	2.6167	1.0356	1.2798	0.5065
		252.49		0.1867	0.0739		
		208.46		3.1000	1.5095		
1	150	206.14	205.36	0.7800	0.3798	1.6757	0.8160
		201.48		3.8800	1.8894		
		168.47		7.3200	4.5424		
	300	165.41	161.15	4.2600	2.6435	4.7822	2.9676
		149.57		11.5800	7.1859		
		251.89		9.3700	3.8636		
	30	234.89	242.52	7.6300	3.1461	4.0694	1.6780
		240.78		1.7400	0.7175		
		205.79		1.4533	0.7112		
3	50	201.48	204.34	2.8567	1.3980	1.1663	0.5708
		205.74		1.4033	0.6868		
		183.49		13.3367	7.8380		
	90	167.49	170.15	2.6633	1.5653	5.7627	3.3868
		159.48		10.6733	6.2728		
		269.49		4.9500	1.8712		
	10	260.41	264.54	4.1300	1.5612	2.1662	0.8189
		263.72		0.8200	0.3100		
		239.13		7.4400	3.2112		
5	20	235.47	231.69	3.7800	1.6315	4.6611	2.0118
		220.47		11.2200	4.8427		
		216.49		9.5767	4.6283		
	30	202.31	206.91	4.6033	2.2248	3.9106	1.8900
		201.94		4.9733	2.4036		

3.2. Thermal Response. The testing results of the thermal response of the basalts induced by microwave irradiation were listed in Table 3. To illustrate the thermal response of the basalts intuitively, the surface temperature of the basalt specimen as a function of the microwave exposure time was shown in Figure 5(a). It is obvious that the surface temperature of the treated basalts increases with the elapsed exposure time linearly. Moreover, with the increase of the microwave power, the heating rate of the basalts increases, while the specimen melts down more quickly. Specially, the cylindrical basalts melt at approximately 221°C in temperature and 300 s in exposure time under power of 1 kW, nearly 215°C in temperature and 100 s in exposure time under power of 3 kW, and almost 155°C in temperature and 50 s in exposure time under power of 5 kW. It concluded that the melting temperature of the basalt obviously decreases as the microwave power increases. The main reason for this is that the rapid heating rate caused by high microwave power can induce temperature gradient and thermal shocks to the compact rocks. In addition, the maximum input microwave energy (calculated from the microwave power and exposure time) in this study is illustrated in Figure 6. The maximum microwave energy absorbed by the basalts exposed at 1 kW, 3 kW, and 5 kW power before fragmentized was approximately 320 kJ, 300 kJ, and 250 kJ, respectively. It indicates that high power density microwave can reduce the energy absorbed competency of the basalts and induce more serious damage induced by the formation of the cracks between or through the mineral particles.

The damage index based on the surface temperature induced by the microwave irradiation can be calculated as follows

$$D_t = \frac{T_0 - T_i}{T_0}, \tag{2}$$

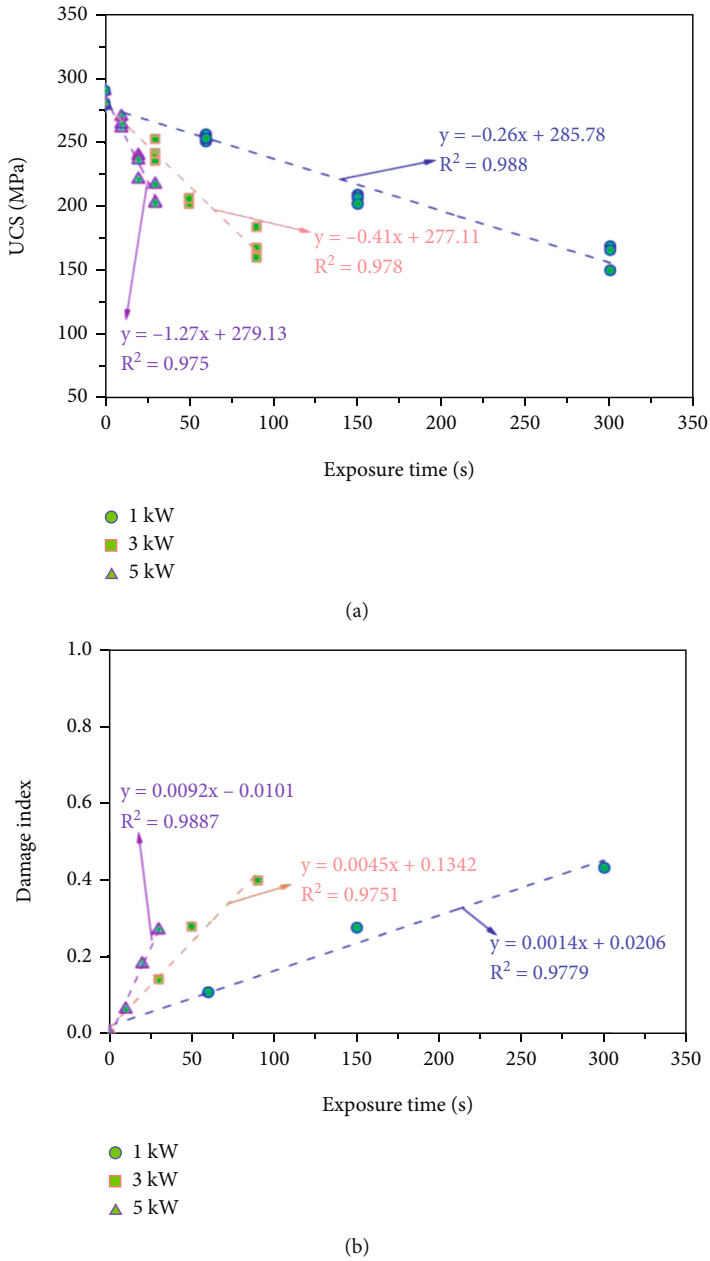

Figure 8: Variation of UCS: (a) UCS of the basalts and (b) damage index based on the UCS.

where D_t is the damage index based on the surface temperature; T_0 is the surface temperature of the basalts nontreated by the microwave; T_i is the surface temperature of the basalts treated by the microwave. Figure 5(b) illustrated the damage index based on the surface temperature of the basalts induced by the microwave irradiation. It can obtain that the damage degree of the basalts induced by the microwave irradiation increases with the elapsed exposure time. Additionally, by comparing the slopes of the fitting curves, the damage degree of the basalts increases rapidly when exposed by high power of microwave. Finally, corresponding to the failure of rocks, the damage index of the basalts induced by the 1 kW, 3 kW, and 5 kW was 8.14, 8.02, and 5.51, respectively. It indicated that the value of damage index based on the thermal response induced by the microwave irradiation was less than 8.2.

3.3. Stress-Strain Curve. Figure 7 illustrates the complete stress-strain curve of basalts specimens before and after microwave irradiated under UCS test.

The stress-strain curve of the original basalts under UCS test can be divided into four stages: (I) the closure stage: the natural defects in the rock close with the load applied and the curve of compact basalts show few closure stage; (II) the liner elastic stage: the curve shows as a straight line and maintains for a period, which occupies nearly 90% of prepeak stage; (III) the yield stage: when the applied load exceeds 90% of peak strength, the curve start shitting to

Table 5: Testing results of elastic modulus induced by microwave irradiation.

Power/kW	Exposure time/s	Elastic modulus/(GPa)	Mean value/(GPa)	Absolute deviation	Relative deviation (%)	Standard deviation/(GPa)	Coefficient of variation (%)
		934.78		2.5433	0.2728		
Nontreated	0	937.18	932.24	4.9433	0.5303	3.1083	0.3334
		924.75		7.4867	0.8031		
		836.49		3.9633	0.4761		
	60	837.02	832.53	4.4933	0.5397	3.4547	0.4150
		824.07		8.4567	1.0158		
		795.48		18.2500	2.3481		
1	150	810.03	777.23	32.8000	4.2201	21.1214	2.7175
		726.18		51.0500	6.5682		
		634.81		23.9933	3.9281		
	300	620.49	610.82	9.6733	1.5837	14.1527	2.3170
		577.15		33.6667	5.5117		
		867.49		10.3067	1.2024		
	30	859.47	857.18	2.2867	0.2668	5.4777	0.6390
		844.59		12.5933	1.4692		
		831.57		11.2433	1.3706		
3	50	815.94	820.33	4.3867	0.5347	4.6268	0.5640
		813.47		6.8567	0.8358		
		705.84		11.1067	1.5987		
	90	697.85	694.73	3.1167	0.4486	6.1044	0.8787
		680.51		14.2233	2.0473		
		915.42		12.1767	1.3481		
	10	906.72	903.24	3.4767	0.3849	6.7114	0.7430
		887.59		15.6533	1.7330		
		867.16		21.6833	2.5646		
5	20	846.79	845.48	1.3133	0.1553	10.5448	1.2472
		822.48		22.9967	2.7200		
		832.95		7.7233	0.9359		
	30	824.24	825.23	0.9867	0.1196	3.4320	0.4159
		818.49		6.7367	0.8163		

the right. Moreover, the rightward shift of curve increases with loading continuously; (IV) the postpeak stage: the basalts failed immediately when the load over than the peak UCS and barely residual strength presents in the postpeak stage. It is concluded that the basalt is a typical type of brittleness rocks.

After microwave irradiation, the stress-strain curves of the basalts show an obvious discrete feature. Specially, following microwave ting, the closure stage of irradiated basalts become extended, while the yield stage shortens. Furthermore, the deformation of the basalts caused by the load mainly consist of elastic deformation of mineral structure and microfracture propagation. After microwave irradiation, the natural fractures between the mineral structures expand, and new defects generate in the mineral particles. Thus, microwave treatment can weaken the bearing capability of the basalts and diminish the extent of rock deformation degree. Finally, deformation capability of the basalts decreases with elapsed microwave irradiation time.

3.4. UCS of Basalt Specimen. The testing results of the UCS of the basalts induced by microwave irradiation were listed in Table 4. To illustrate the UCS variation of the basalts intuitively, the UCS of the basalt specimen as a function of the microwave exposure time was shown in Figure 8(a). It is easily obtained that microwave irradiation can be able to weaken the bearing capability of the compact basalts. When exposed by the microwave at 1 kW power for 300 s, the peak strength of the basalts declined to 161.09 MPa, while that of the nontreated specimen was 282.93 MPa. The UCS of the basalts treated at 3 kW for 90 s and at 5 kW for 30 s was 170.38 MPa and 206.79 MPa, respectively. It suggests that the degrees of UCS reduction are significantly influenced by the input microwave energy, which can be concluded by the microwave power and irradiation time. Moreover, the UCS of treated basalts presents a linear decrease relationship with the exposure time, and by comparing the slopes of the linear fitting curves, high microwave power can result in a large extent of UCS reduction rate. It can be concluded that the microwave power and irradiation time are vertical

Table 6: Testing results of Poisson's ratio induced by microwave irradiation.

Power/kW	Exposure time/s	Poisson's ratio	Mean value	Absolute deviation	Relative deviation (%)	Standard deviation	Coefficient of variation (%)
		0.288		0.0027	0.9346		
Nontreated	0	0.279	0.2853	0.0063	2.2196	0.0026	0.9099
		0.289		0.0037	1.2850		
		0.2826		0.0028	0.9887		
	60	0.2815	0.2798	0.0017	0.5956	0.0018	0.6534
		0.2754		0.0044	1.5843		
		0.2811		0.0089	3.2823		
1	150	0.2706	0.2722	0.0016	0.5756	0.0039	1.4310
		0.2648		0.0074	2.7067		
		0.2734		0.0085	3.2088		
	300	0.2538	0.2649	0.0111	4.1903	0.0047	1.7894
		0.2675		0.0026	0.9815		
		0.2816		0.0014	0.4877		
	30	0.2832	0.2802	0.0030	1.0586	0.0018	0.6455
		0.2759		0.0043	1.5463		
		0.271		0.0023	0.8435		
3	50	0.2715	0.2687	0.0028	1.0295	0.0021	0.7659
		0.2637		0.0050	1.8730		
		0.2649		0.0074	2.8871		
	90	0.2518	0.2575	0.0057	2.2009	0.0032	1.2315
		0.2557		0.0018	0.6862		
		0.283		0.0047	1.6766		
	10	0.281	0.2783	0.0027	0.9581	0.0030	1.0889
		0.271		0.0073	2.6347		
		0.259		0.0057	2.2368		
5	20	0.252	0.2533	0.0013	0.5263	0.0024	0.9549
		0.249		0.0043	1.7105		
		0.251		0.0019	0.7627		
	30	0.2351	0.2491	0.0140	5.6202	0.0062	2.4892
		0.2612		0.0121	4.8575		

parameters effecting the mechanical performance of the basalt rock.

The damage index based on the UCS induced by the microwave irradiation can be calculated as follows:

$$D_s = \frac{\sigma_0 - \sigma_i}{\sigma_0}, \tag{3}$$

where D_s is the damage index based on the UCS; σ_0 is the UCS of the basalts nontreated by the microwave; σ_i is the UCS of the basalts treated by the microwave. Figure 8(b) illustrated the damage index based on the UCS of the basalts induced by the microwave irradiation. It can obtain that the damage degree of the basalts induced by the microwave irradiation increases with the exposure time increases. Additionally, by comparing the slopes of the fitting curves, the damage degree of the basalts increases rapidly when exposed by high power of microwave. Finally, corresponding to the failure of rocks, the damage index of the basalts induced by the 1 kW, 3 kW, and 5 kW was 0.43, 0.39, and 0.27, respectively. It indicated that the value of damage index based on the UCS induced by the microwave irradiation was less than 0.45.

3.5. Mechanical Constants. Elastic modulus and Poisson's ratio were two crucial parameters to investigate the correlation between compression deformation and applied loads and can be calculated by the straight-line segment of the stress-strain curves. The testing results of the elastic modulus and Poisson's ratio of the basalts induced by microwave irradiation were listed in Tables 5 and 6, respectively. To illustrate the mechanical constants of the basalts intuitively, the elastic modulus and Poisson's ratio of the basalt specimen as a function of the microwave exposure time were shown in Figures 9(a) and 9(c), respectively. It is obtained that the original basalt is a type of hard and compact rocks with approximately 932.4 GPa in elastic modulus. However, by the microwave irradiation, the elastic modulus and

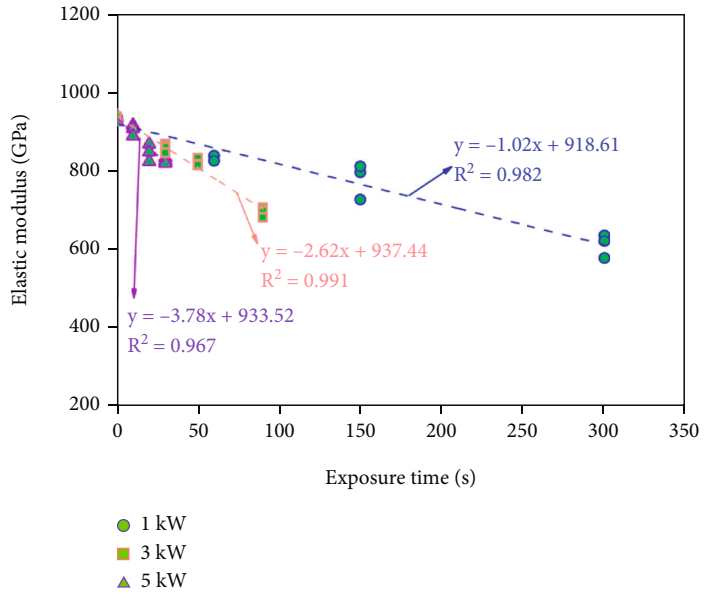

(a)

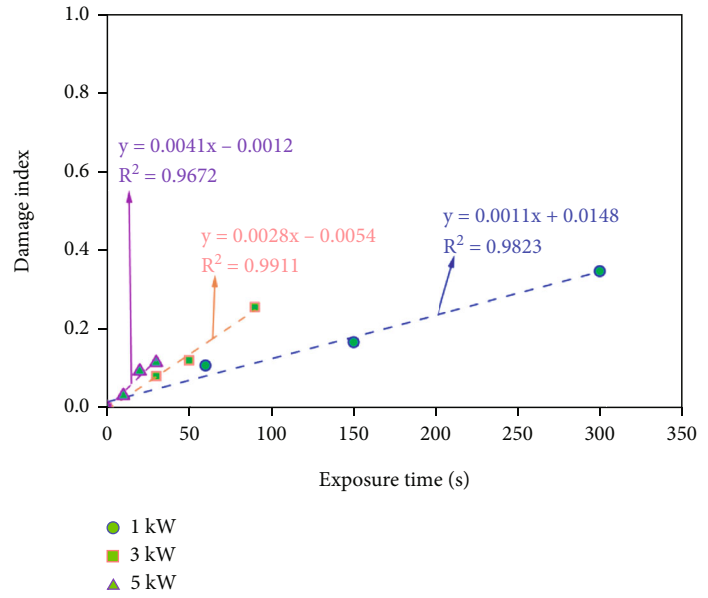

(b)

Figure 9: Continued.

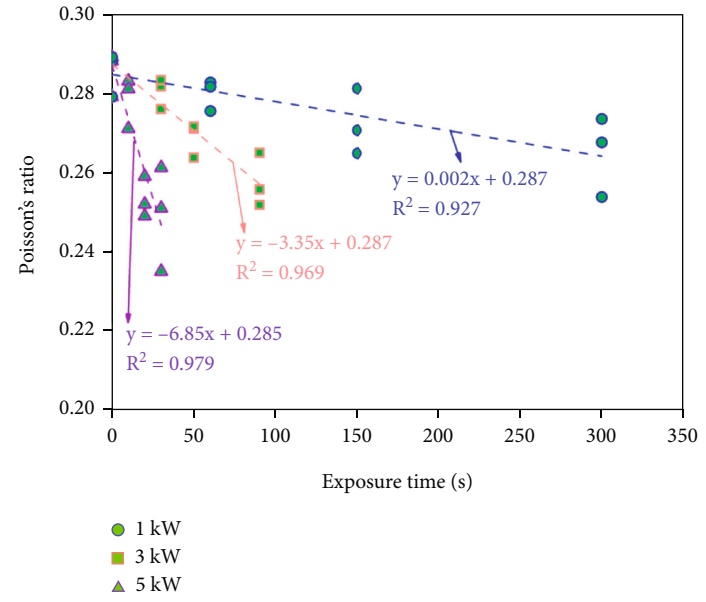

(c)

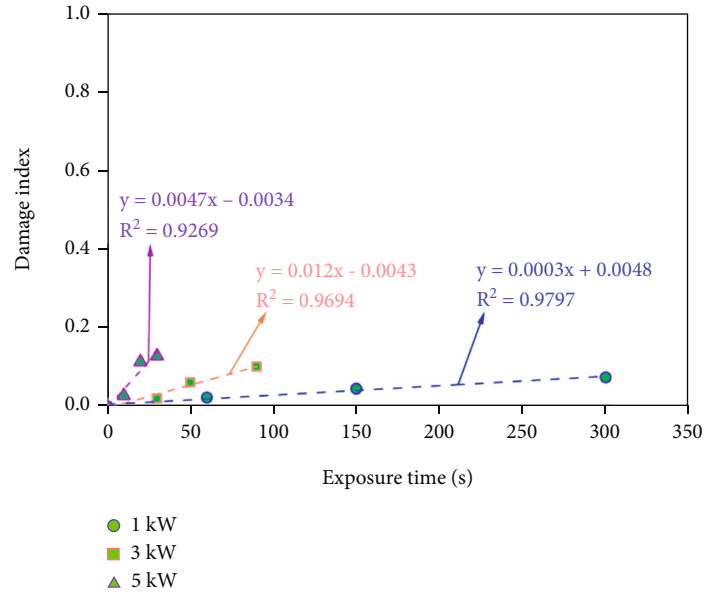

(d)

Figure 9: Variation of mechanical constants: (a) elastic modulus of the basalts, (b) damage index based on the elastic modulus, (c) Poisson's ratio of the basalts, and (d) damage index based on the Poisson's ratio.

Poisson's ratio of the basalts decrease obviously. Typically, the elastic modulus and Poisson's ratio can be both characterized by linear fitting curves on the exposure time. Furthermore, high microwave power will induce a large extent of the reduction rate of elastic modulus and Poisson's ratio.

The damage index based on the elastic modulus and Poisson's ratio induced by the microwave irradiation can be calculated as follow, respectively:

$$D_E = \frac{E_0 - E_i}{E_0}, \tag{4}$$

$$D_P = \frac{\lambda_0 - \lambda_i}{\lambda_0}, \tag{5}$$

where D_E is the damage index based on the elastic modulus; E_0 is the elastic modulus of the basalts nontreated by the microwave; E_i is the elastic modulus of the basalts treated by the microwave. D_P is the damage index based on the Poisson's ratio; λ_0 is the Poisson's ratio of the basalts nontreated by the microwave; λ_i is the Poisson's ratio of the basalts treated by the microwave. Figures 9(b) and 9(d) illustrated the damage index based on the elastic modulus and Poisson's ratio of the basalts induced by the microwave irradiation, respectively. It can obtain that the damage degree of

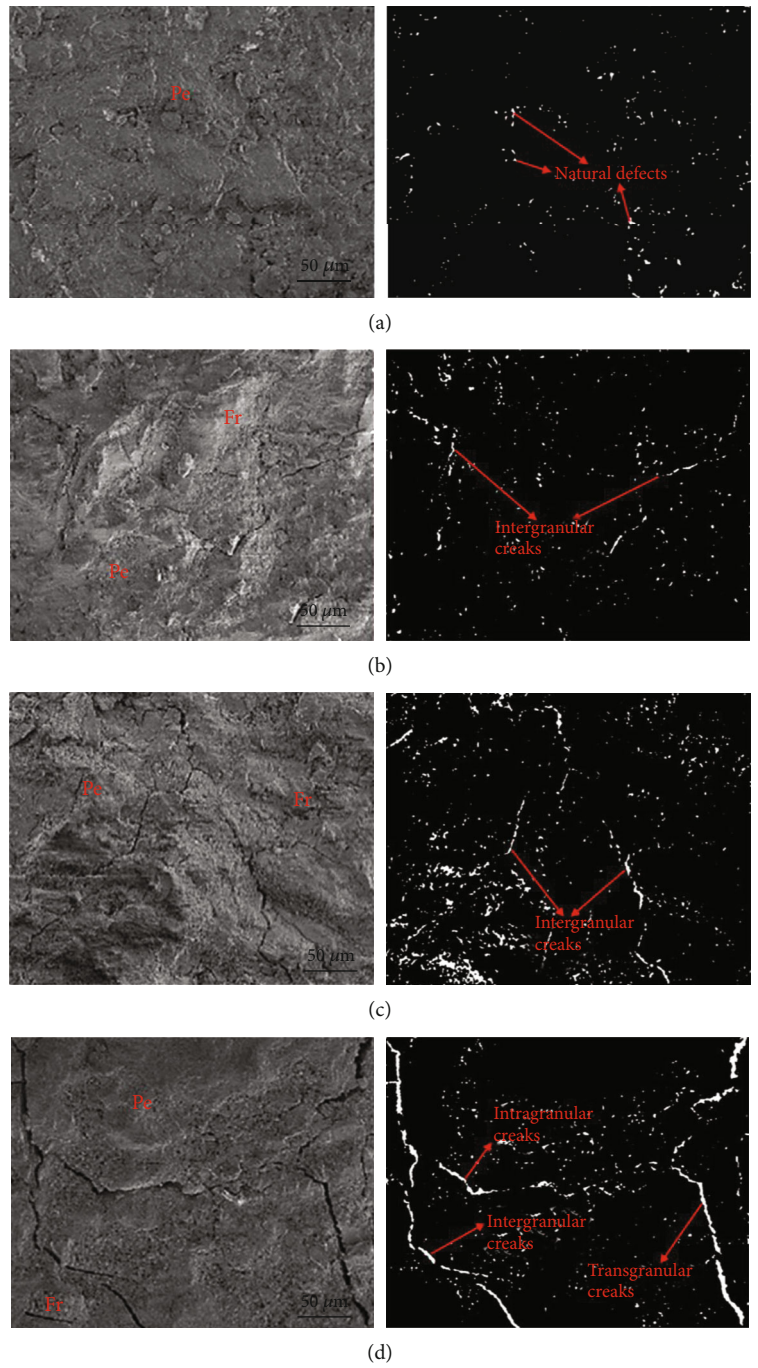

Figure 10: SEM images of basalts: (a) nontreated, (b) exposed at 5 kW for 10 s, (c) exposed at 3 kW for 90 s, and (d) exposed at 1 kW for 300 s.

the basalts induced by the microwave irradiation increases with the elapsed exposure time. Additionally, by comparing the slopes of the fitting curves, the damage degree of the basalts increases rapidly when exposed by high power of microwave. Finally, the maximum of the damage index of the basalts based on the elastic modulus induced by the 1 kW, 3 kW, and 5 kW was 0.35, 0.26, and 0.12, respectively. It indicated that the value of damage index based on the elastic modulus induced by the microwave irradiation was less than 0.4. Meanwhile, the maximum of the damage index of the basalts based on the Poisson's ratio induced by the 1 kW, 3 kW, and 5 kW was 0.07, 0.11, and 0.13, respectively. It indicated that the value of damage index based on the Poisson's ratio induced by the microwave irradiation was less than 0.15.

4. Discussion

4.1. SEM Analysis. Figure 10 reveals the SEM images and morphology of microcracks of the basalts before and after

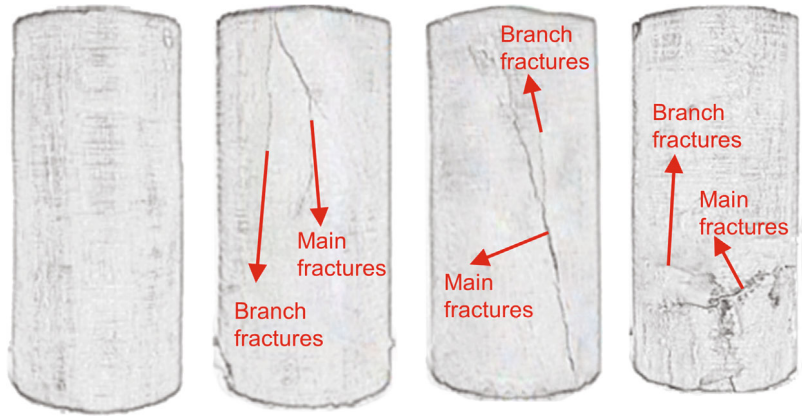

Figure 11: Geological sketches of the basalts (a) before irradiation and after exposed at (b) 1 kW, (c) 3 kW, and (d) 5 kW for 20 s.

microwave irradiation. All types of cracks (i.e., intergranular cracks, transgranular cracks, and intragranular cracks) can be identified, and the patterns of the microcracks are signed by arrows in the figure. Figure 7(a) shows that the mineral particles were complete, and a few of natural cracks between grain boundaries exist in the nontreated basalts. However, when the basalts were treated at power of 5 kW for 10 s, intergranular cracks in the rocks generated along the grain boundary between pyroxene and feldspar are as shown in Figure 7(b). Besides, it can be easily observed from Figure 7(c) that the intergranular crack growth in length and the distance between the mineral particles approximately tripled induced by the microwave irradiation at 3 kW for 90 s. Furthermore, mixed-mode cracks consist of all types of microcracks generated after the basalts were exposed for 300 s by the 1 kW microwave and a dominant crack extended rapidly to induce macrofracture in the basalt specimen as shown in Figure 7(d). It is indicated that the patterns of the microcracks induced by the microwave irradiation in the basalts were advanced developed with the microwave energy constantly input. The significant difference heating rate of the mineral particles involved in the basalts induces temperature gradient. The different thermal deformation of the grain from each other result in the mutual extrusion and thermal stress between the mineral particles, and hence, macrofractures can occur as the microwave irradiation time elapsed.

4.2. Macrofracture Propagation Pattern. Microwave irradiation by generating a series of microcracks could induce contactless damages to weaken the strength of compact rocks. The higher the level of microwave power and the longer the treating time, the more inner microcracks generated and propagated by the microwave irradiation. Furthermore, visible macrofracture networks in the treated rocks would format by the connectivity and anastomosis of the inducing defects. Figure 11 shows the various morphologies of the fracture networks in the basalts induced by the microwave irradiation. It can be observed that the fracture network consists of main fractures and branch fractures. Main fractures increase the depth of the fracture networks, and branch fractures around the main fractures improve the network width, both of which weaken the strength of rocks. By comparing Figures 11(a) and 11(b), the depth of the main fractures increases from approximate half of the specimen length to two-thirds of that exposed for 20 s, while the variation of the branch fractures is not evident. Meanwhile, when microwave power is below 3 kW, the fracture propagation follows the direction of the central axis of the cylindrical specimen. However, when the power level increases to 5 kW, the pattern of the fracture propagation changes completely. For the main fractures, the direction rotated from axial to circumferential, and then, the branch propagation pattern transformed from along the direction of the main fracture to vertical with that. Specially, compared with low power microwave, high power density microwave can be able to evidently decrease the depth of fracture network, while width of that obviously increases. This reaction suggests that the macrofracture propagation pattern could be exchanged by applying different power microwave.

5. Conclusions

In this research, a series of physical and mechanical experiments were conducted on the cylindric basalts to investigate the thermal response and mechanical behaviors of compact rocks induced by microwave irradiation. Research results were concluded as follows:

(1) The transmission velocity of the ultrasonic wave applied on the exposed basalts was significantly influenced by the microwave power and heating time. More serious degradation of the P-wave velocity could be induced by the higher level of microwave power and the longer of heating time. The decreasing dependence of P-wave velocity on the microwave power and heating time can be reflected by various linear fitting line

(2) Intergranular cracks, transgranular cracks, and intragranular cracks were observed by SEM, and the macrofracture propagation pattern of the basalts

exposed at different power levels was obtained by geological sketch. With the constantly exposed by the microwave, newly defects generated and inducing microcracks coalesced to form the main fractures and branch fractures. Moreover, the propagation direction of the visible macrofractures rotated from axial to circumferential by apply different powers of microwave, and higher power microwave could induce the fracture propagate shorter, while more extensive in width

(3) The UCS and elastic constants of the basalts present negative relationship with the microwave power and exposure time. The UCS of basalts declined to 161.09 MPa at 1 kW for 300 s, decreases to 170.38 MPa after treated by 3 kW power microwave for 90 s, and drops to 206.79 MPa at 5 kW for 30 s, respectively. Moreover, the mechanical performance of the treated basalts is significantly influenced by the input microwave energy, which is dominated by power level and treating time

Data Availability

The data used to support the findings of this study are included within the article.

Conflicts of Interest

The authors declare that they have no conflicts of interest.

Acknowledgments

This paper was supported by the Independent Research Project of State Key Laboratory of Coal Resources and Safe Mining, CUMT (Grant number SKLCRSM2020X05) and the Key projects of the Joint Fund of the National Natural Science Foundation of China (Grant number U21A20107).

References

[1] B. Maidl, L. Schmid, W. Ritz, and M. Herrenknecht, *Hardrock Tunnel Boring Machines*, Wiley, New York, America: New York, 2008.

[2] K. Bäppler, "New developments in TBM tunnelling for changing grounds," *Tunnelling and Underground Space Technology*, vol. 57, pp. 18–26, 2016.

[3] Y. L. Zheng, Q. B. Zhang, and J. Zhao, "Challenges and opportunities of using tunnel boring machines in mining," *Tunnelling and Underground Space Technology*, vol. 57, pp. 287–299, 2016.

[4] W. S. Li, B. Y. Jiang, S. T. Gu, X. X. Yang, and F. U. A. Shaikh, "Experimental study on the shear behavior of grout-infilled specimens and micromechanical properties of grout-rock interface," *Journal of Central South University*, vol. 29, no. 5, pp. 1686–1700, 2022.

[5] Q. Gong, L. Yin, H. Ma, and J. Zhao, "TBM tunnelling under adverse geological conditions: an overview," *Tunnelling and Underground Space Technology*, vol. 57, pp. 4–17, 2016.

[6] L. Home, "Hard rock TBM tunneling in challenging ground: developments and lessons learned from the field," *Tunnelling and Underground Space Technology*, vol. 57, pp. 27–32, 2016.

[7] A. K. M. Jamaluddin, L. M. Vandamme, and B. K. Mann, *Formation Heat Treatment (FHT): A State-of-the-Art Technology for Near-Wellbore Formation Damage Treatment*, The Petroleum Society of CIM, 1995.

[8] A. K. M. Jamaluddin, M. Hamelin, K. Harke, H. McCaskill, and S. A. Mehta, "Field testing of the formation heat treatment process," *Journal of Canadian Petroleum Technology*, vol. 38, no. 3, pp. 38–45, 1999.

[9] Q. Feng, J. Jin, S. Zhang, W. Liu, X. Yang, and W. Li, "Study on a damage model and uniaxial compression simulation method of frozen–thawed rock," *Rock Mechanics and Rock Engineering*, vol. 55, no. 1, pp. 187–211, 2022.

[10] S. Jamali, V. Wittig, J. Börner, R. Bracke, and A. Ostendorf, "Application of high powered laser technology to alter hard rock properties towards lower strength materials for more efficient drilling, mining, and geothermal energy production," *Geomechanics for Energy and the Environment*, vol. 20, p. 100112, 2019.

[11] R. Fuxin and Z. Gaofeng, "Experimental and numerical investigation of laser-induced rock damage and the implications for laser-assisted rock cutting," *International Journal of Rock Mechanics and Mining Sciences*, vol. 139, p. 104653, 2021.

[12] R. Taheri, M. Kabuli, and Z. Vryzas, "Fracturing and permeability enhancement with laser technology employing fuzzy logic," *Journal of Petroleum Science and Engineering*, vol. 188, no. C, p. 106830, 2020.

[13] V. R. Ikkurthi, K. Tahiliani, and S. Chaturvedi, "Simulation of crack propagation in rock in plasma blasting technology," *Shock Waves*, vol. 12, no. 2, pp. 145–152, 2002.

[14] V. F. Vazhov, S. Y. Datskvich, M. Y. Zhurkov, and V. M. Muratov, "Electric pulse breakdown and rock fracture in a coupled environment of increased pressure and temperature," *Journal of Physics Conference Series*, vol. 552, no. 1, pp. 012050–012054, 2014.

[15] S. M. Razavian, B. Rezai, and M. Irannajad, "Investigation on pre-weakening and crushing of phosphate ore using high voltage electric pulses," *Advanced Powder Technology*, vol. 25, no. 6, pp. 1672–1678, 2014.

[16] A. R. Llera, A. Díaz, F. J. Pedrayes, J. M. Menéndez-Aguado, and M. G. Melero, "Study of comminution kinetics in an electrofragmentation lab-scale device," *Metalsmith*, vol. 12, no. 3, p. 494, 2022.

[17] K. Teimoori and R. Cooper, "Multiphysics study of microwave irradiation effects on rock breakage system," *International Journal of Rock Mechanics and Mining Sciences*, vol. 140, p. 104586, 2021.

[18] M. Toifl, P. Hartlieb, R. Meisels, T. Antretter, and F. Kuchar, "Numerical study of the influence of irradiation parameters on the microwave- induced stresses in granite," *Minerals Engineering*, vol. 103-104, pp. 78–92, 2017.

[19] P. Hartlieb, B. Grafe, T. Shepel, A. Malovyk, and B. Akbari, "Experimental study on artificially induced crack patterns and their consequences on mechanical excavation processes," *International Journal of Rock Mechanics and Mining Sciences*, vol. 100, pp. 160–169, 2017.

[20] V. Becattini, T. Motmans, A. Zappone, C. Madonna, A. Haselbacher, and A. Steinfeld, "Experimental investigation of the thermal and mechanical stability of rocks for high-

temperature thermal-energy storage," *Applied Energy*, vol. 203, pp. 373–389, 2017.

[21] H. Sun, Q. Sun, W. Deng, W. Zhang, and C. Lü, "Temperature effect on microstructure and P-wave propagation in Linyi sandstone," *Applied Thermal Engineering*, vol. 115, pp. 913–922, 2017.

[22] F. Hassani, P. M. Nekoovaght, and N. Gharib, "The influence of microwave irradiation on rocks for microwave-assisted underground excavation," *Journal of Rock Mechanics and Geotechnical Engineering*, vol. 8, no. 1, pp. 1–15, 2016.

[23] G. Lu, Z. Sun, J. Zhou, K. Chen, and F. Li, "Effect of microwave irradiation on computed tomography and acoustic emission characteristics of hard rock," *Geotechnical and Geological Engineering*, vol. 39, no. 1, pp. 411–424, 2021.

[24] J. Lu, H. Xie, M. Li et al., "Effect of microwave radiation on mechanical behaviors of tight fine sandstone subjected to true triaxial stress," *International Journal of Rock Mechanics and Mining Sciences*, vol. 152, p. 105063, 2022.

[25] X. B. Zhao, Q. H. Zhao, Q. M. Gong, and J. L. He, "Preliminary study on the weakening effect of microwave irradiation on Singapore Bukit Timah granite and its influence on mechanical excavation performance," *Geomechanics and Geophysics for Geo-Energy and Geo-Resources*, vol. 8, no. 4, p. 110, 2022.

[26] Z. Ge and Q. Sun, "Acoustic emission characteristics of gabbro after microwave heating," *International Journal of Rock Mechanics and Mining Sciences*, vol. 138, p. 104616, 2021.

[27] T. Xu, L. He, Y. Zheng, X. Zou, V. Badrkhani, and D. Schillinger, "Experimental and numerical investigations of microwave-induced damage and fracture formation in rock," *Journal of Thermal Stresses*, vol. 44, no. 4, pp. 513–528, 2020.

[28] Q. H. Zhao, X. B. Zhao, Y. L. Zheng et al., "Heating characteristics of igneous rock-forming minerals under microwave irradiation," *International Journal of Rock Mechanics and Mining Sciences*, vol. 135, p. 104519, 2020.

[29] S. Kahraman, A. N. Canpolat, and M. Fener, "The influence of microwave treatment on the compressive and tensile strength of igneous rocks," *International Journal of Rock Mechanics and Mining Sciences*, vol. 129, p. 104303, 2020.

[30] C. E. Fairhurst and J. A. Hudson, "Draft ISRM suggested method for the complete stress-strain curve for intact rock in uniaxial compression," *International Journal of Rock Mechanics and Mining Sciences*, vol. 36, no. 3, pp. 279–289, 1999.